Ni-, Pd-, or Pt-catalyzed ethylene dimerization: a mechanistic description of the catalytic cycle and the active species†

Dipankar Roy and Raghavan B. Sunoj*

Received 14th October 2009, Accepted 20th November 2009
First published as an Advance Article on the web 11th January 2010
DOI: 10.1039/b921492e

Two key mechanistic possibilities for group 10 transition metal $[M(\eta^3\text{-allyl})(PMe_3)]^+$ catalyzed (where M = Ni(II), Pd(II) and Pt(II)) ethylene dimerization are investigated using density functional theory methods. The nature of the potential active catalysts in these pathways is analyzed to gain improved insights into the mechanism of ethylene dimerization to butene. The catalytic cycle is identified as involving typical elementary steps in transition metal-catalyzed C–C bond formation reactions, such as oxidative insertion as well as β-H elimination. The computed kinetic and thermodynamic features indicate that a commonly proposed metal hydride species (L_nM–H) is less likely to act as the active species as compared to a metal–ethyl species (L_nM–CH_2CH_3). Of the two key pathways considered, the active species is predicted to be a metal hydride in pathway-1, whereas a metal alkyl complex serves as the active catalyst in pathway-2. A metal-mediated hydride shift from a growing metal alkyl chain to the ethylene molecule, bound to the metal in an η^2 fashion, is predicted to be the preferred route for the generation of the active species. Among the intermediates involved in the catalytic cycle, metal alkyls with a bound olefin are identified as thermodynamically stable for all three metal ions. In general, the Ni-catalyzed pathways are found to be energetically more favorable than those associated with Pd and Pt catalysts.

Introduction

In the last decade, several organic synthesis methodologies have become available that have placed considerable importance on atom economy, as well as green chemistry approaches.[1] The demands for high purity compounds and materials for healthcare, as well as device applications, have witnessed a steady increase. In general, one strives to translate the maximum number of atoms in the raw material into the desired product, while keeping other requisite substances only to catalytic amounts. The classic examples that satisfy the atom economy criteria include catalytic hydrogenation[2] and the Diels–Alder reaction.[3] While the recent developments in organocatalytic reactions[4] have been perceived as successful in achieving dependable stereoselectivity, higher catalyst loading continues to be one of the general issues. On the other hand, the arena of transition metal catalysis is known to be effective in being atom economic. Understanding how different reagents are transformed into products in transition metal-catalyzed reactions is of fundamental importance. Improved insights on the reaction mechanism could serve to optimize the reaction conditions, design new catalysts, and also to exploit the potential of such reactions.

Among the several related developments in C–C bond formation methodologies, the transition metal-catalyzed reactions enjoy a special significance.[5] The most commonly employed catalysts contain transition metal(s) nested in suitably designed ligand(s).[6] Homogeneous organometallic catalysts offer a large array of reactivity, tunability (by means of varying the metal/ligand) as well as high catalytic efficiency. Impressive selectivity in C–C bond-forming reactions has also been achieved using transition metal catalysts.[7] From a mechanistic viewpoint, computational studies[8] on some of the popular reactions such as the Heck reaction,[9] hydroformylation,[10] hydrovinylation[6c,11] and alkene polymerization[12] are available. In an alkene dimerization reaction, as shown in Scheme 1, the metal complex is typically treated with the alkene in the presence of a Lewis acid co-catalyst (LA) to generate a *pre-catalyst*, which enters the catalytic cycle. The central transition metal in the pre-catalyst is often ligated with P- or N-containing ligands.[13] The reverse process, *i.e.* metal-catalyzed C–C bond cleavage, is less likely to happen under ordinary conditions due to the inertness of the carbon–carbon σ-bonds towards metals.

It is generally suggested that a metal hydride complex serves as the active catalyst in alkene dimerization.[14] The debate over the existence of a true active catalyst is not well-settled to date.[15] When a high level of alkene concentration is maintained, the survival of a metal hydride complex as the active catalyst is less likely. Instead, an alkylated metal complex is expected to act as the active catalyst.[16] The possible involvement of a metal alkyl complex as the active catalyst brings about two key mechanistic pathways. These possibilities, designated as pathways-1 and -2, are illustrated in Scheme 2, with the help of a representative example of the group 10 transition metals, a Ni-catalyzed ethylene dimerization reaction.

Perusal of the recent literature reveals that studies directed towards addressing the nature of the active catalysts is not widely present.[14b,17] While the attempts towards isolation and detection of metal alkyl species in cross-coupling and co-polymerization

Department of Chemistry, Indian Institute of Technology Bombay, Powai, Mumbai 400076, India. E-mail: sunoj@chem.iitb.ac.in; Fax: +91-22-2576-7152

† Electronic supplementary information (ESI) available: The mPW1K/LANL2DZ, 6-311+G** optimized coordinates and energies of stationary points involved in the Ni(II), Pd(II) and Pt(II) catalytic cycles; B3LYP/LANL2DZ, 6-311+G** and PBE1PBE/LANL2DZ, 6-311+G** optimized coordinates and energies of the transition states of Ni(II)-catalyzed reactions. See DOI: 10.1039/b921492e

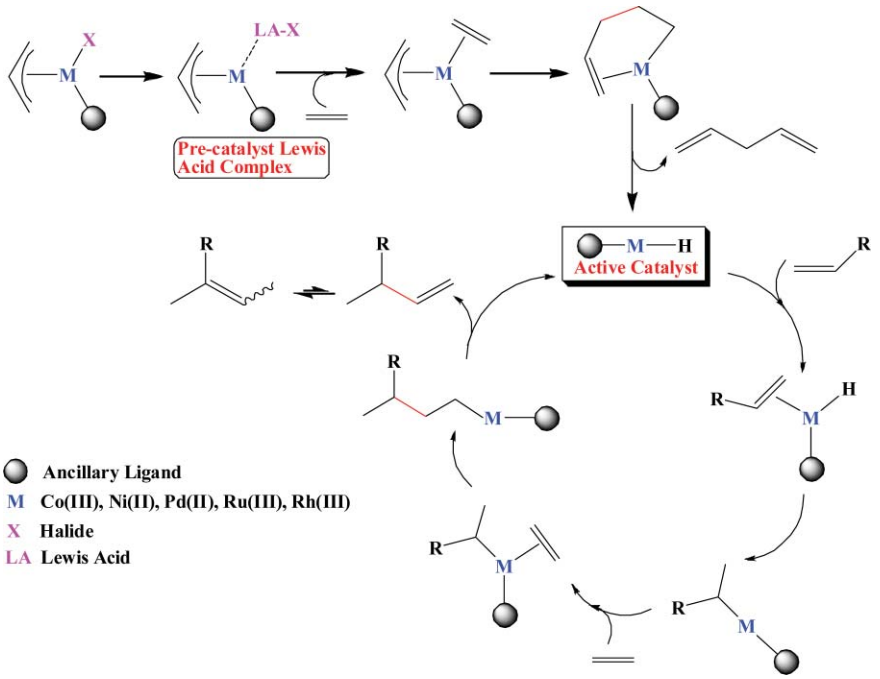

Scheme 1 The generally proposed mechanism for transition metal-catalyzed alkene dimerization (charge on the metal is not shown for clarity).

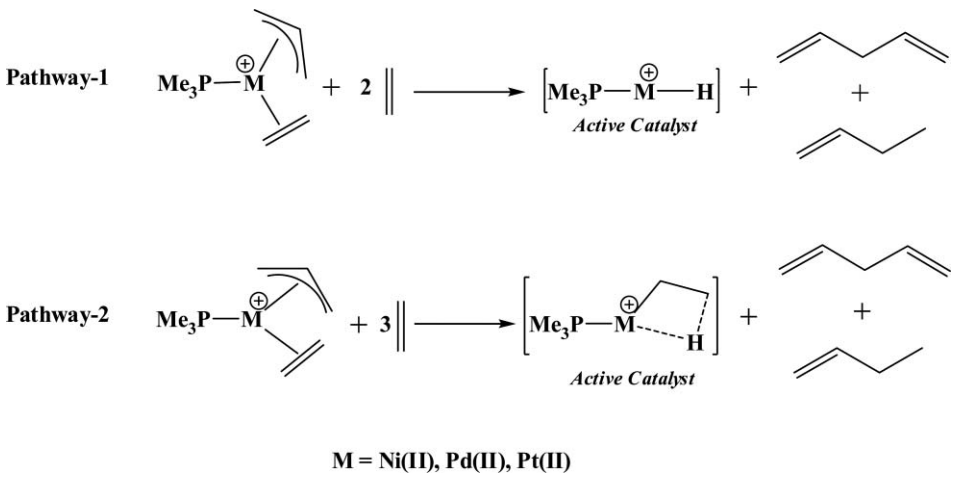

Scheme 2 Two key pathways for ethylene dimerization catalyzed by Ni-group transition metal complexes. The active catalysts in pathways-1 and -2 are proposed as a metal hydride and a metal alkyl species, respectively.

reactions are known,[18] insights on the nature of the active species in Ni/Pd/Pt-catalyzed ethylene dimerization are not available to the best of our knowledge. Furthermore, most of the related studies have employed bidentate ligands, instead of a monodentate phosphine ligand. Considering the importance of Ni-, Pd- and Pt-catalyzed reactions in organic chemistry, the mechanistic insights on carbon–carbon or carbon–heteroatom bond formation reactions are indeed quite valuable.[19] In the present study, we intend to (i) shed light on two plausible mechanistic pathways, hitherto unexplored, in the case of ethylene dimerization, and (ii) probe the nature of the active catalyst on the basis of the computed energetics. The approach includes detailed analysis of structural and energetic features of important intermediates and transition states associated with each elementary step in the catalytic cycle. Since the involvement of the active catalyst is a general feature of transition metal-mediated olefin polymerization, the results could have wider implications towards providing improved understanding on this important homogeneous catalytic process.

Computational methods

All calculations were carried out using the Gaussian03 suite of quantum chemical programs.[20] The hybrid density functional mPW1K was primarily employed in the present study.[21] The zero-point vibrational energy corrections and thermal corrections were applied to the "bottom-of-the-well" values to obtain enthalpy ($H_{298\,K}$) and Gibbs free energy ($G_{298\,K}$). These computations assume the standard state as 1 atmospheric pressure. Additional

calculations with hybrid functionals, such as B3LYP[22] and PBE1PBE,[23] were also used to re-evaluate the activation energies for the Ni(II)-catalyzed reaction cycles. The LANL2DZ basis set, consisting of an effective core potential (ECP) for 36 electrons (Kr core) and Hay–Wadt's valence basis functions for all other electrons, was employed for Ni, Pd, and Pt.[24] The rest of the elements were represented by Pople's basis set, 6-311+G**. The success of the B3LYP functional is well-documented in the context of modeling chemical reactions involving transition metal catalysis.[25] The choice of the mPW1K functional is also guided by the literature reports on its successful applications in organometallic chemistry.[26] The PBE1PBE functional is also known to yield reliable energetics for transition metal systems, in particular, for those involving agostic interactions.[27]

The nature of stationary points was first verified by the visual inspection of the imaginary frequencies as pertaining to the desired reaction coordinate. The transition states were characterized by one and only one imaginary frequency representing the reaction coordinate. Furthermore, the intrinsic reaction coordinate (IRC) analysis was performed to authenticate the transition states.[28] The natural bond orbital (NBO) analysis was performed at the mPW1K level in combination with the LANL2DZ basis set for metals and the 6-311+G** basis set for all other atoms.[29] The topological analysis of the electron density using the wave function generated at the mPW1K/LANL2DZ, 6-311+G** level of theory was carried out within the *Atoms in Molecules* (AIM) formalism, as implemented in the AIM2000 program.[30] This enabled us to understand the key bond paths and the electron densities at the corresponding bond critical points.

To reduce additional computational costs, the larger aryl groups on the phosphine ligands were replaced by methyl groups (PMe_3) in the present study. The discussions in the text employ the computed Gibbs free energies in the gas phase obtained by including unscaled zero-point vibrational energy, as well as thermal corrections, to the *bottom-of-the-well* energy values. The activation parameters are reported with respect to $[M(C_3H_5)(PMe_3)]^+$ and the appropriate number of ethylene molecule(s) involved in the respective elementary steps (where M = Ni, Pd or Pt).

Results and discussion

The transition metal catalyst $[M(\eta_3\text{-allyl})(PPh_3)]^+$ with labile ligands, such as chloride, has been found to be of use, as a starting point, for several catalytic processes. In fact, $[(C_3H_5)Pd(PPh_3)]Cl$ itself is a commercially available compound. Under homogeneous conditions, the reaction is typically initiated by the generation of an active Pd(II) pre-catalyst (**2a**), by replacing the labile ligand with an olefin. In the present study, a detailed investigation of the catalytic cycle by considering each step associated with olefin dimerization, starting from the pre-catalyst, is undertaken. The Gibbs free energy, and the electronic structure features of various transition states and intermediates involved in the two key mechanistic pathways, differing in the nature of the active catalysts, as well as the corresponding catalytic cycle, are described in the following sections. All energies reported herein are obtained at the mPW1K level, unless otherwise stated.[31] The detailed discussions are presented first for Ni, and then for both Pd and Pt. Lastly, a comparative account of their catalytic cycles is provided.

1. Ni-catalyzed ethylene dimerization

(i) Pathway-1, involving Ni hydride as the active catalyst. The first step in the dimerization involves the complexation of ethylene with $[(C_3H_5)Ni(PMe_3)]^+$ (**1a**) to yield a 16e species **1b**. This process is found to be highly favored thermodynamically (ΔH_{rxn} and ΔG_{rxn} are −25.8 and −13.2 kcal mol^{-1}, respectively). In the next step, a facile C–C bond formation between the allyl and ethylene molecules bound to the Ni(II) occurs through the involvement of transition state **TS(1b–1c)**, leading to a nickel pentenyl intermediate **1c**, as shown in Scheme 3. The key structural parameters for these stationary points are highlighted in the optimized geometries provided in Fig. 1. The Ni–P bond in **TS(1b–1c)** is found to be shorter (2.18 Å) than both in **1b** (2.24 Å) and in product **1c** (2.21 Å). This geometric feature is identified as arising due to the improved electron donation from the σ-donating PMe_3 ligand to nickel in **TS(1b–1c)**, as compared to that in the reactant and the product.[32] It is important to note at this juncture that the first key difference between the two major catalytic cycles begins with intermediate **1c**. The mechanistic course is going to be different if further olefin uptake by **1c** is considered (*vide infra*). On the other hand, the cycle can continue through the conversion of **1c** to **1d**, as described below. A rotation around the Ni–C_{alkyl} bond in **1c** results in intermediate **1d**. The relative Gibbs free energy of **TS(1c–1d)** and the corresponding free energy of activation for this step are found to be about 7 and 20 kcal mol^{-1}, respectively. It is worth noting that the olefinic coordination of Ni is lost due to this rotation. The optimized geometry of **1d** conveys the presence of a β-agostic interaction (*vide infra*).[33] A low energy transition state for the conversion of **1d** to **1d′**, with a nearly linear P–Ni–C_{alkyl} disposition is also identified.

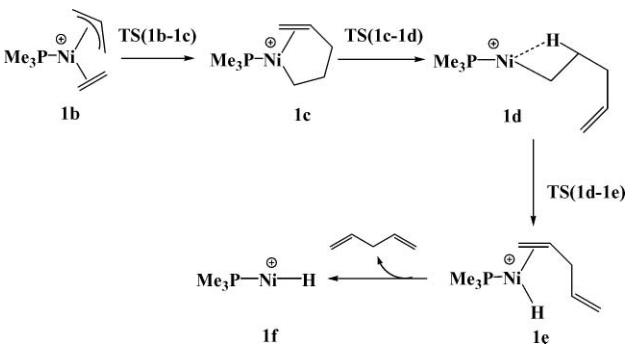

Scheme 3 Mechanism of generation of the nickel hydride active catalyst in Ni(II)-catalyzed ethylene dimerization through pathway-1.

In the next step, an intramolecular β-H elimination in **1d′** leads to the formation of a nickel hydride complex (**1e**). The corresponding transition state, **TS(1d′–1e)**, is predicted to possess a slightly higher Gibbs free energy than the first two steps in the catalytic pathway.[34] The release of 1,4-pentadiene by **1e** furnishes the coordinatively unsaturated nickel hydride species **1f**, participation of the same in the catalytic cycle is generally debated.[35] The generation of this putative intermediate is identified as highly endergonic, with a free energy of reaction (ΔG_{rxn}) as high as 53.8 kcal mol^{-1}. The unstable metal hydride is expected to serve as the *active catalyst* for the subsequent steps in the catalytic cycle.[36] A logical connection between this prediction and intractable experimental difficulties associated with the detection of such

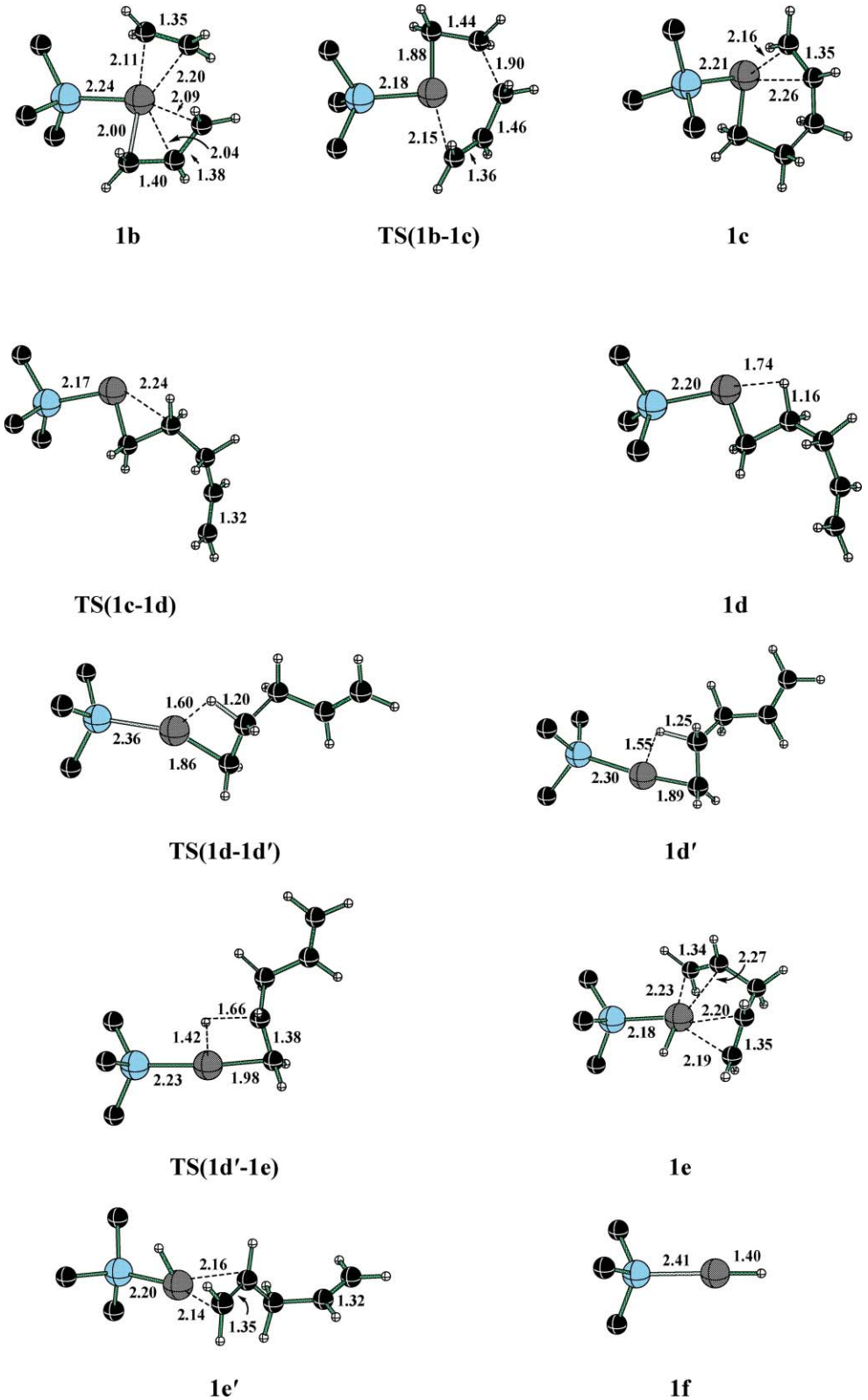

Fig. 1 The mPW1K/LANL2DZ, 6-311+G** optimized geometries of important transition states and intermediates in the nickel-catalyzed ethylene dimerization reaction (bond lengths in Å). Color code: gray–Ni; cyan–P; black–C; ivory–H.

active catalysts in related oligomerization reactions deserves due consideration here. The identification of such active catalysts has remained largely elusive, presumably owing to the large endoergicity of formation, as noted above. The formation of **1f** is quite unfavorable, primarily due to the loss of stabilization provided by metal $\cdots\pi$ interaction(s), which is present in the other preceding intermediates.

Soon after the active catalyst **1f** is generated, uptake of a molecule of ethylene can lead to intermediate **1g**. The major driving force for this step comes from the π-complexation between ethylene and Ni. With this, a catalytic cycle kicks in, as shown in Scheme 4. It is interesting to note that the π-complex **1g** is about 42 kcal mol^{-1} more stable than the reactive intermediate **1f**, implying a very high propensity for olefin uptake by **1f**. In the subsequent step, a hydride transfer to the ethylene moiety through **TS(1g–1h)** results in metal alkyl complex **1h**.[37] The structural details of **1h** indicate the presence of an activated C–H bond at the free end of ethylene (Fig. 2). The presence of activated C–H bonds arising due to β-agostic interaction in organometallic complexes is well-documented in the literature.[38] The relatively higher-energy intermediate **1h** can now take another ethylene molecule to yield a more stable π-complex **1i**. The next crucial step is the C–C bond formation between the ethyl and ethylene fragments bound to Ni. The optimized geometry of the transition state for the C–C bond formation, **TS(1i–1j)**, is provided in Fig. 2. The resulting Ni–butyl complex **1j** occupies an interesting position on the free energy profile, as another olefin uptake would lead to a mechanistic bifurcation toward pathway-2. More importantly, **1j** is the first reasonably stable intermediate ($\Delta G = -16.8$ kcal mol^{-1}) identified on the reaction profile (Fig. 2).

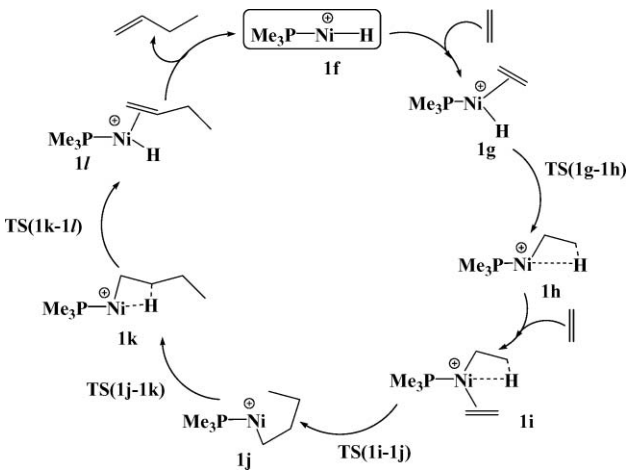

Scheme 4 Proposed catalytic cycle for ethylene dimerization involving pathway-1, centered around a 'nickel hydride' active catalyst.

Along pathway-1, a low barrier torsional motion of the butyl group in **1j** is identified. Through this torsional transition state, **TS(1j–1k)**, another key intermediate, **1k**, with an activated β C–H bond is generated. This intermediate can undergo a relatively low barrier β-H transfer to yield another catalytically active Ni hydride species **1l**. In the final step of the catalytic cycle, product 1-butene is expelled, along with the regeneration of the active species **1f**.[39] The cycle continues by further olefin uptake, as shown in Scheme 4. Thus far, the discussions have been revolving around the catalytic cycle, wherein a high-energy nickel hydride species plays the key role of active catalyst. In the next section, discussion on another potential active catalyst is presented.

(ii) Pathway-2, involving Ni alkyl species as the active catalyst. While the first step in this pathway is identical to that of pathway-1, two key differences are evident. The first point of difference relates to the uptake of a second molecule of ethylene by intermediate **1c** to yield **1m**, as shown in Scheme 5. Considering the easy availability of the olefin under generally employed experimental conditions, such as high olefin pressures,[40] **1c** to **1m** conversion appears quite likely. In fact, the Gibbs free energy is predicted to be relatively more favorable for the formation of the bis-olefin intermediate **1m**. The generation of an alkylated pre-catalyst, **1n**, through an intramolecular hydride transfer involving **TS(1m–1n)** is unique to this pathway. More interestingly, **TS(1m–1n)** exhibits a Ni-mediated shuttling of the hydrogen atom. A reasonably strong interaction is noticed between the transferring hydrogen atom and the nickel center.[41] The optimized transition state geometries of the key stationary points are provided in Fig. 3. The subsequent release of 1,4-pentadiene from **1n** provides a metal alkyl species, **1h**, which triggers the catalytic cycle as shown in Scheme 6. The species **1h** can be thought of as a point of convergence between the two plausible catalytic pathways (pathways-1 and -2). It is interesting to note that **1h** could also be obtained from **1g**, described earlier in pathway-1. Both catalytic pathways therefore share intermediates **1h**, **1i** and **1j**. The major difference between pathways-2 and -1 pertains to the nature of the active species involved in the catalytic cycle. In pathway-2, the active species is a nickel alkyl complex (**1h**) with an activated β-C–H bond, whereas a nickel hydride (**1f**) serves as the active catalyst in pathway-1.

The reaction sequence continues to be the same as in pathway-1, up until Ni butyl complex **1j**. Akin to the conversion of **1c** to **1m** described earlier, uptake of another olefin is quite likely by the coordinatively unsaturated **1j**. The resulting intermediate, with an ethylene bound to Ni in an η^2-fashion (**1o**), is found to be exergonic by about –28 kcal mol^{-1}. The computed relative stability indicates that **1o** could be amenable to interception/detection through appropriately designed experimental techniques.

In the final phase of the catalytic cycle, the C_β–H from the butyl moiety is transferred to ethylene. The Gibbs free energy of activation indicates a relatively lower barrier for the conversion of **1o** to **1p**. The analysis of the corresponding transition state, **TS(1o–1p)**, as provided in Fig. 3, indicates that the nickel is facilitating a hydride transfer. The resulting complex **1p**, which is equivalent to an active catalyst, consists of a metal alkyl species with a bound 1-butene. Finally, the release of 1-butene regenerates the active catalyst **1h**, which is expected to keep the catalytic cycle alive.

A complete list of the relative energies of various transition states for different elementary steps is provided in Table 1 and a graphical illustration of the same is given in Fig. 4. It is important at this juncture to point out that the barriers associated with pathway-2 are, in general, lower than those observed in the pathway leading to the formation of the active catalyst **1f** in pathway-1. In fact, in pathway-2, the rotation of the Ni-bound pentenyl unit *via* **TS(1c–1d)** is identified as the highest energy transition state on the free energy profile. Even more noteworthy, is that the intermediates involved in pathway-2 are relatively more stable compared to those in pathway-1. The computed Gibbs free

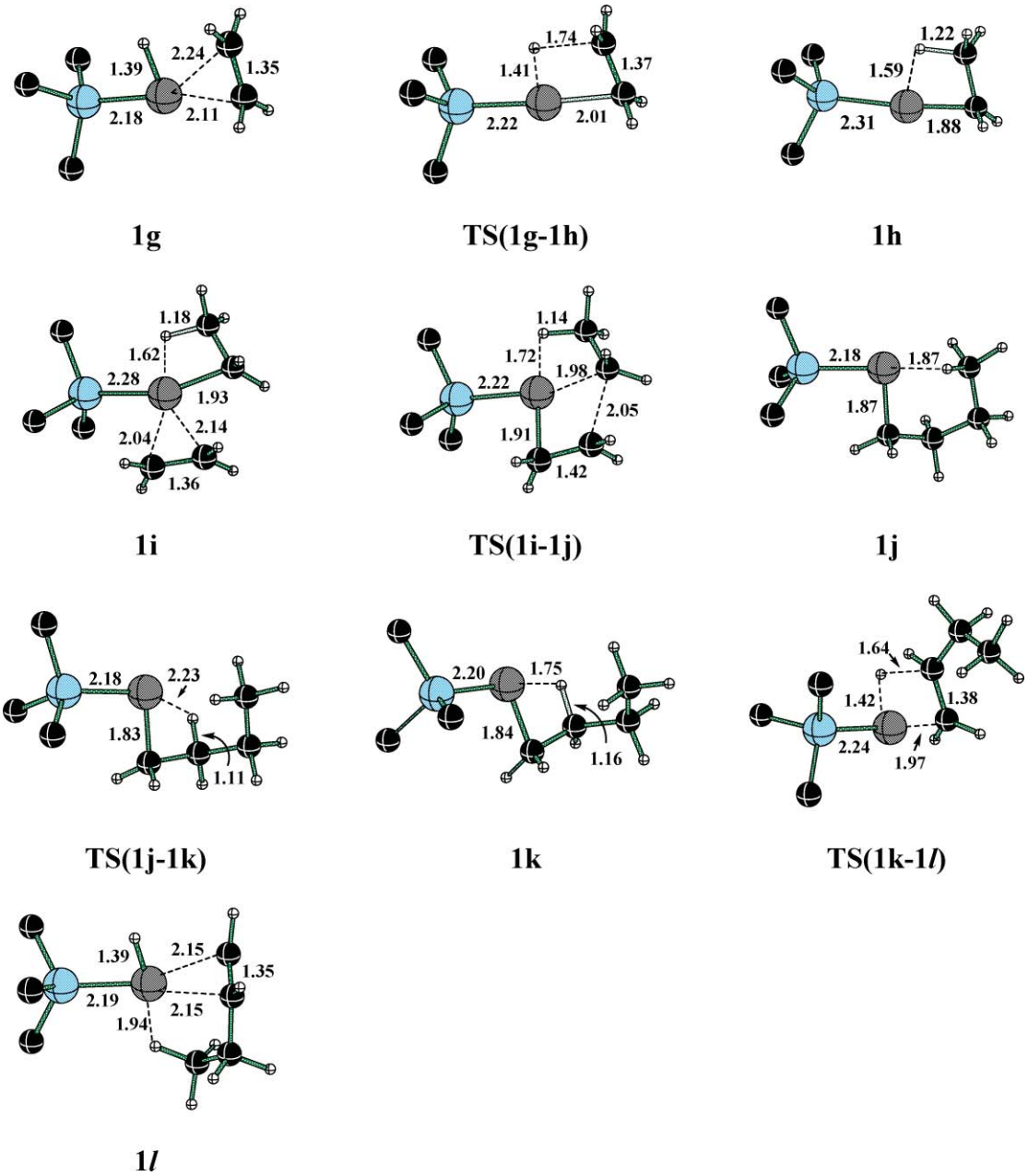

Fig. 2 The mPW1K/LANL2DZ, 6-311+G** optimized geometries of important transition states and intermediates in the ethylene dimerization reaction (bond lengths in Å) involving nickel hydride as the active catalyst, as depicted in Scheme 4 (pathway-1). Color code: gray–Ni; cyan–P; black–C; ivory–H.

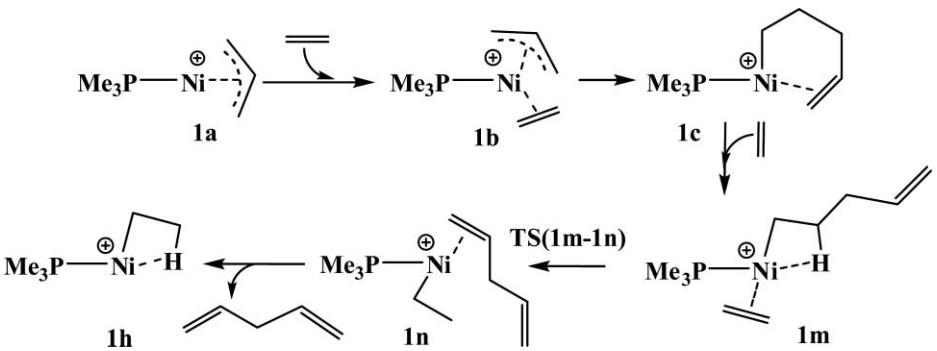

Scheme 5 Mechanism of generation of nickel alkyl 'active catalyst' in Ni(II)-catalyzed ethylene dimerization through pathway-2.

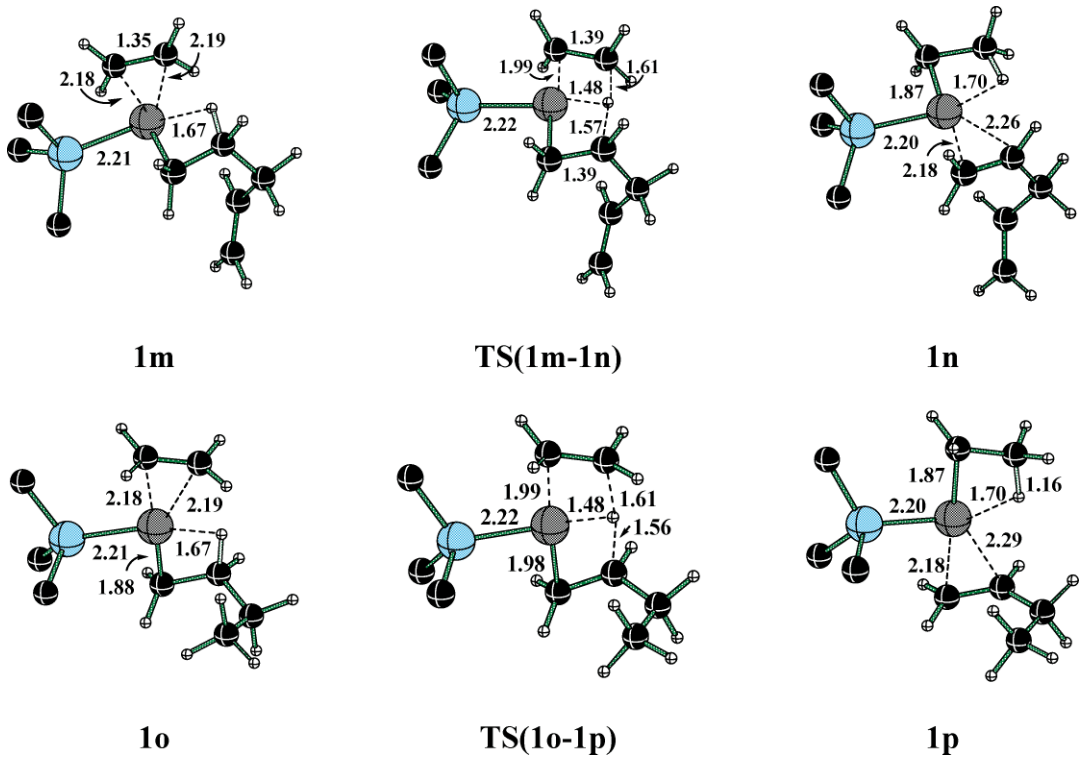

Fig. 3 The mPW1K/LANL2DZ, 6-311+G** optimized geometries of important transition states and intermediates (bond lengths in Å). Color code: gray–Ni; cyan–P; black–C; ivory–H.

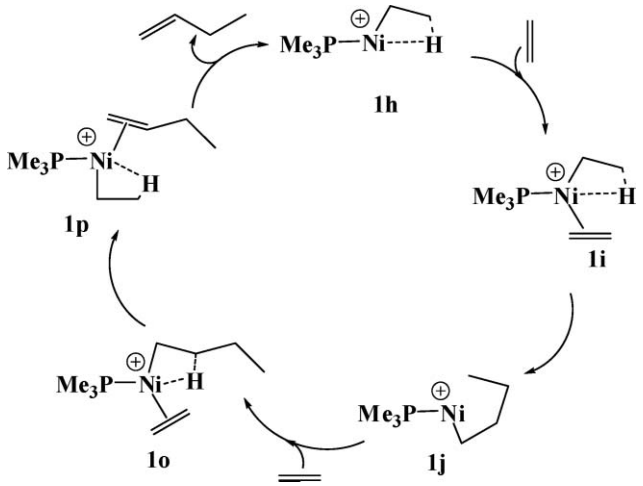

Scheme 6 Proposed catalytic cycle of ethylene dimerization involving pathway-2 centered around a nickel alkyl active species.

Table 1 Relative energies[a] (in kcal mol^{-1}), obtained at the mPW1K level of theory, for the key transition states involved in pathway-1 and pathway-2 for ethylene dimerization

Transition state	ΔH			ΔG		
	Ni(II)	Pd(II)	Pt(II)	Ni(II)	Pd(II)	Pt(II)
b–c	−17.0	−5.3	−8.9	−3.4	9.1	4.6
c–d	−4.6	−12.0	−9.7	6.8	1.31	2.7
d–d′	3.2	—[b]	—[b]	13.9	—[b]	—[b]
d–e	1.2	0.4	4.3	12.1	12.8	14.1
g–h	3.2	2.0	5.5	13.3	13.4	15.3
i–j	−28.0	−16.3	−16.1	−4.8	7.5	7.3
j–k	−37.2	−39.3	−37.1	−14.3	−15.6	−14.2
k–l	−29.0	−23.9	−26.0	−7.1	−0.4	−2.4
m–n	−28.3	−22.2	−32.1	−4.0	2.6	−7.7
o–p	−57.6	−51.6	−61.4	−22.4	−15.8	−26.3
e–f′	—[c]	−5.2	−13.9	—[c]	7.1	-−2.3
l–r	−32.6	—[b]	—[b]	−10.2	—[b]	—[b]

[a] Relative energies are with respect to **a** and the appropriate number of ethylene and pentadiene molecule(s). [b] Identified only in Ni-catalyzed reactions. [c] Not associated in the Ni-catalyzed dimerization.

energies suggest that the formation of metal alkyl intermediates with a bound olefinic fragment, such as **1m**, **1n**, **1o** and **1p**, are quite feasible (Fig. 4). Suitably designed detection/trapping experiments directed towards these intermediates could, therefore, be able to shed light in understanding the nature of the resting state as well as the catalytically active species.

2. Pd(II)-catalyzed ethylene dimerization

In this section, the details on Pd-catalyzed ethylene dimerization are presented. Since elaborate description of various elementary steps for the Ni-catalyzed pathways has been provided in the previous sections, discussions here are primarily confined towards highlighting the key differences between Ni- and Pd-catalyzed ethylene dimerization pathways.

Similar to the Ni-catalyzed process, the first step in the Pd(II)-catalyzed pathway is the uptake of an ethylene molecule by the cationic pre-catalyst $[(C_3H_5)Pd(PMe_3)]^+$ (**2a**) to yield the 16e complex **2b**. This process is found to be highly favorable, both in terms of enthalpy and Gibbs free energy ($\Delta H_{rxn} = -24.6$ kcal mol^{-1}, and

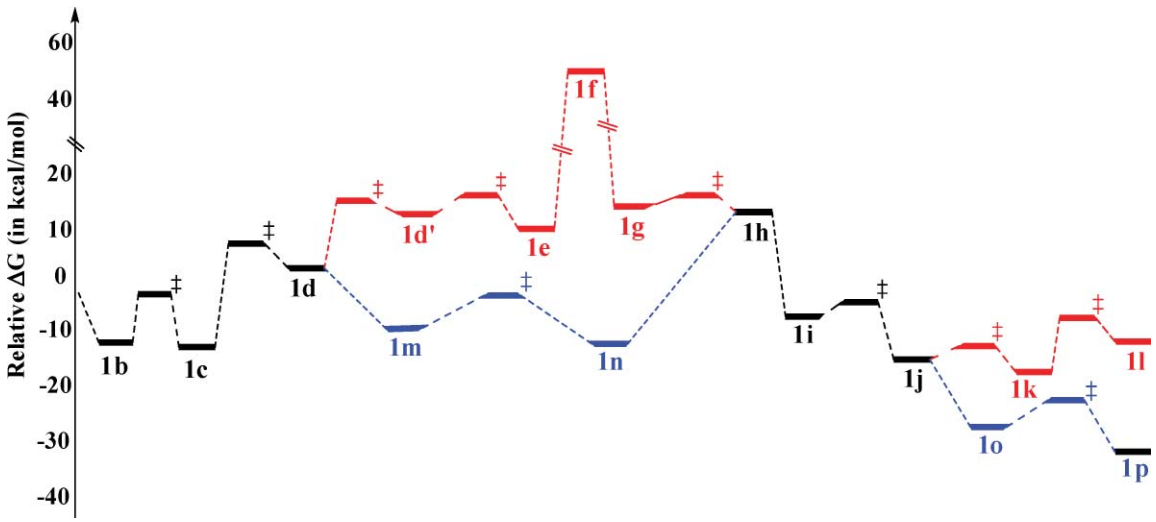

Fig. 4 The reaction profile constructed using the Gibbs free energies, obtained at the mPW1K level of theory, for Ni(II)-catalyzed ethylene dimerization. (Elementary steps common to both the pathways are in black, while those associated exclusively with pathway-1 and pathway-2 are, respectively, in red and blue colours.)

$\Delta G_{rxn} = -11.3$ kcal mol^{-1}). The prediction that the generation of **2b** is exothermic is consistent with an available experimental report, wherein the presence of a cationic $[(C_3H_5)Pd(C_2H_4)PCy_3]^+$ intermediate is confirmed by low temperature NMR measurements.[42] In the next step, the allyl and ethylene groups bound to the Pd(II) pre-catalyst **2b** undergo C–C bond formation through **TS(2b–2c)**, leading to a palladium pentenyl intermediate **2c** (similar to Scheme 5). A subsequent low energy rotational transition state converts intermediate **2c** to **2d**. The intermediate **2e**, obtained by walking down from the corresponding transition state **TS(2d–2e)**, exhibits η^2 coordination by both olefinic ends of the pentadiene. The expulsion of pentadiene from **2e** is identified to proceed through a two-step process. First, the weaker η^2 Pd$\cdots\pi$ bond at one end of the pentadiene opens up through **TS(2e–2f′)** to yield intermediate **2f′**, which is about 13 kcal mol^{-1} higher in energy than the bis η^2 Pd$\cdots\pi$ complex **2e** ($\Delta G_R = 11.4$ kcal mol^{-1}). The subsequent steps in pathway-1 for the Ni(II) and Pd(II) catalytic pathways are found to be similar in nature.

The activation barriers for most of the elementary steps associated with pathway-2 in the Pd(II)-catalyzed reaction are comparatively higher than those predicted for the corresponding Ni(II)-catalyzed steps. The geometrical features are found to be

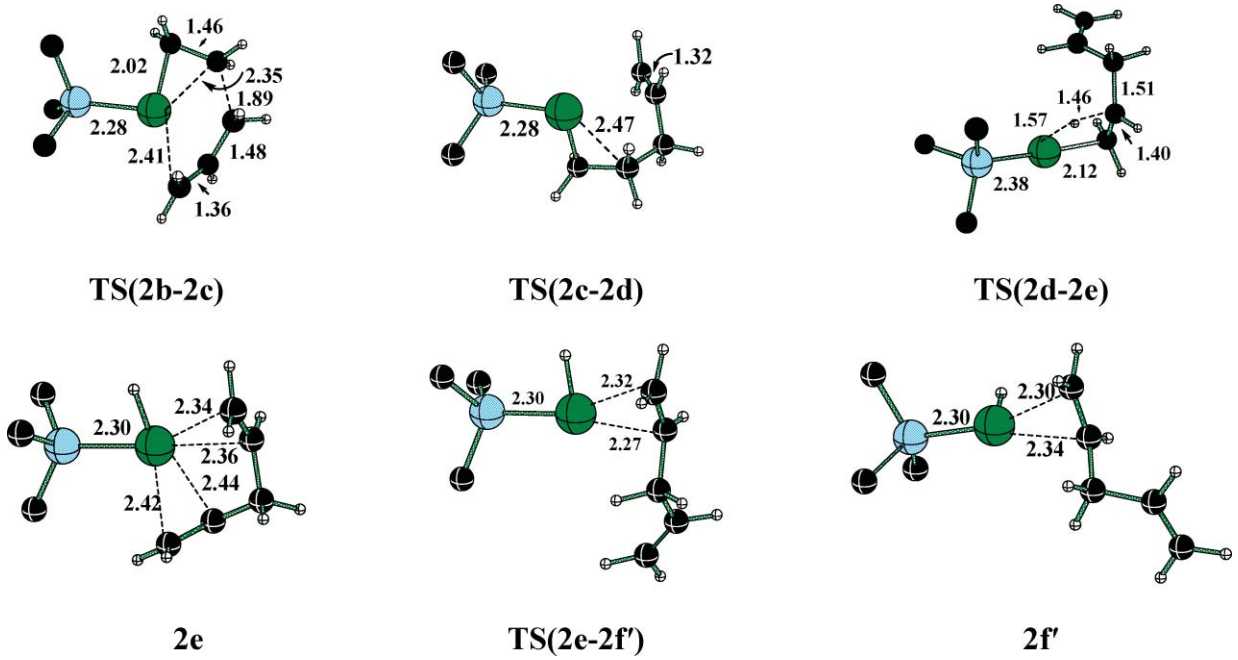

Fig. 5 The mPW1K/LANL2DZ, 6-311+G** optimized geometries of important transition states and intermediates in palladium-catalyzed ethylene dimerization reaction (bond lengths in Å). Color code: green–Pd; cyan–P; black–C; ivory–H.

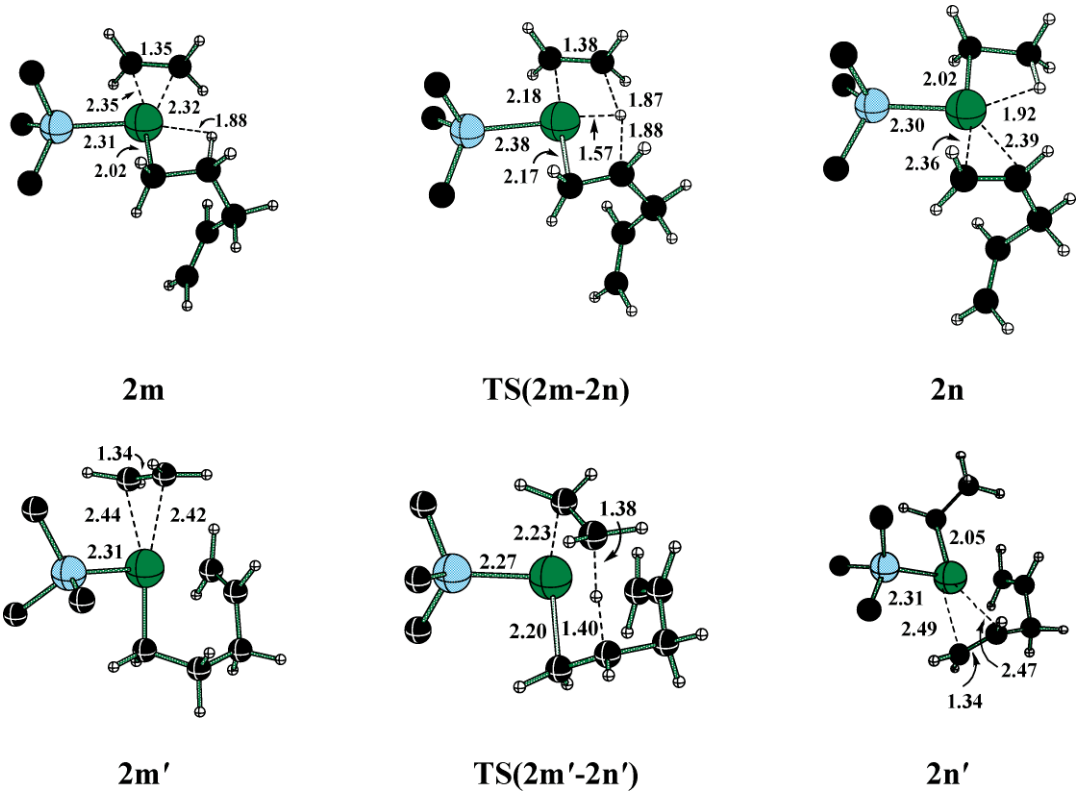

Fig. 6 The mPW1K/LANL2DZ, 6-311+G** optimized geometries of important transition states and intermediates (bond lengths in Å). Color code: green–Pd; cyan–P; black–C; ivory–H.

generally similar in both of these cases (see Fig. 5 and 6). However, an additional transition state for the hydride transfer, **TS(2m′–2n′)**, is identified, where the preceding intermediate (**2m′**) exhibits an additional Pd $\cdots\pi$ interaction with the pentadiene, akin to that in intermediate **2e** (see Fig. 5 and 6). However, this transition state is found to be significantly higher in energy ($\Delta H_{rel} = 6.9$ and $\Delta G_{rel} =$ 33.6 kcal mol^{-1}) than **TS(2m–2n)**.[43]

3. Pt(II)-catalyzed ethylene dimerization and comparison with the lighter congeners

The overall features of the Pt(II)-catalyzed ethylene dimerization are found to be similar to those predicted for the lighter analogues, Pd(II) and Ni(II).[44,45] The C–C bond formation between the allyl and ethylene moieties through **TS(3b–3c)** is identified as the rate-limiting step in pathway-2. The inspection of the overall reaction profile, as given in Fig. 7, helps to establish this more clearly.[46] As with the lighter congeners, the platinum hydride species, **3f** in pathway-1, is found to be a high-energy active species.

A comparison between the catalytic cycles of all three transition metals reveals several interesting facts. First, in pathway-1, the metal hydride intermediate is found to be the highest energy species on the respective potential energy surfaces. The metal hydride generation of platinum $[(Me_3P)Pt–H]^+$ appears to be relatively less favored compared to the other two metal hydrides.[47] Interestingly, the activation parameters of the hydride transfer step, as revealed by the energies of **TS(1g–1h)**, **TS(2g–2h)** and **TS(3g–3h)**, convey a higher barrier in the case of platinum. The comparison of different elementary steps, in general, suggests that the nickel-catalyzed pathways exhibit lower activation barriers.

For a number of intermediates and transition states for the Ni(II) system, the presence of a stabilizing Ni $\cdots$ H_β agostic interaction is identified. The heavier congeners, *i.e.* Pd and Pt, on the other hand, enjoy stabilization arising from additional M $\cdots\pi$ interactions. These indicate that **2g** and **3g** are likely candidates to act as the resting state in the catalytic cycles involving Pd and Pt. However, the rate-limiting step is found to be different in the nickel-catalyzed process compared to that with palladium and platinum. While the rate-limiting step involves the conversion of **1c** to **1d** in the case of nickel, it is identified as the first C–C bond formation (**2b–2c** and **3b–3c**) for palladium and platinum.[48]

Another general feature of various intermediates along the catalytic pathways is the presence of agostic interactions. In particular, intermediates **d**, **h**, **i**, **j**, **k**, **n** and **p** exhibit metal $\cdots$ H_β agostic interactions, as is evident from the elongated C–H_β bonds.[49] In all of these intermediates, a moderate to large increase in the C–H bond length is noticed. Moreover, the bond critical points are identified using the topological analysis of the electron density, within the atoms-in-molecules formulation, between the metal atom and the H-atom involved in the β-agostic interaction.[33] The magnitude of the computed electron density at these (agostic) bond critical points is found to be higher than that reported for normal hydrogen bonds.[50]

One more interesting aspect that we have examined in this study pertains to the relative performance of two density functionals towards capturing the essential features of the potential energy surfaces. The results presented thus far have been obtained using

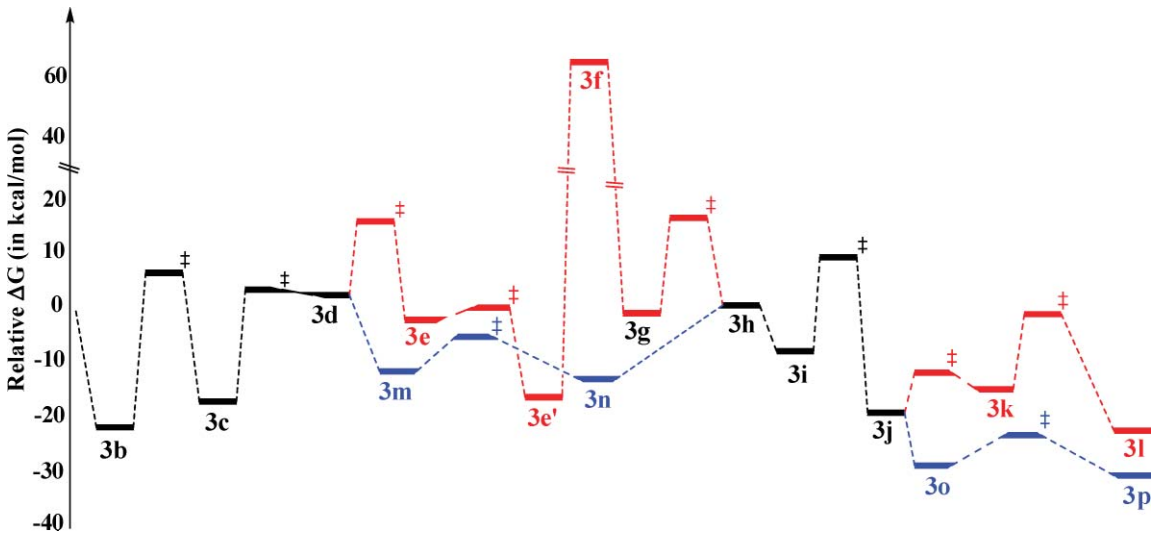

Fig. 7 The reaction profile constructed using the Gibbs free energies obtained at the mPW1K level of theory for Pt(II)-catalyzed ethylene dimerization. (Elementary steps common to both the pathways are in black, while those associated exclusively with pathway-1 and pathway-2 are in red and blue colours, respectively.)

Table 2 Relative energies[a] (in kcal mol^{-1}), obtained at the B3LYP level of theory, for the key transition states involved in pathway-1 and pathway-2 for Ni(II)-catalyzed ethylene dimerization

	B3LYP		PBE1PBE	
Transition state	ΔH	ΔG	ΔH	ΔG
1b–1c	–9.4	4.1	–19.6	–6.2
1c–1d	–4.3	7.8	–4.5	6.5
1d–1e	6.6	17.3	1.5	12.0
1g–1h	8.2	17.0	3.3	12.3
1i–1j	–14.2	6.8	–29.4	–7.6
1j–1k	–22.6	–1.2	–36.4	–14.7
1k–1l	–14.8	5.6	–28.0	–7.3
1m–1n	–16.4	6.8	–32.2	–8.5
1o–1p	–37.8	–4.3	–60.8	–27.1

[a] Computed enthalpies and free energies (in kcal mol^{-1}) are relative to species **1a** and the suitable number of ethylene molecules.

the mPW1K functional. There have been reports on the successful applications of other density functionals in organometallic reactivity problems. In particular, hybrid functionals such as B3LYP and PBE1PBE are widely employed in related studies.[27,51] In order to examine how the mPW1K results compare with other popularly employed functionals, we have calculated the activation parameters using both the B3LYP and PBE1PBE functionals. The details of the calculated energetics are provided in Table 2. The predicted barriers, as well as relative stabilities of the key intermediates computed using the PBE1PBE functional, are found to be in good agreement with those obtained at the mPW1K level. The computed relative energies at the B3LYP level are found to be generally higher than those reported with some of the related examples.[52]

Conclusion

Two important mechanistic possibilities for Ni(II)-, Pd(II)- and Pt(II)-catalyzed cationic ethylene dimerization have been studied using the density functional theory methods. The involvement of a metal hydride species (pathway-1) or a metal alkyl species (pathway-2) as the 'active catalyst' is compared on the basis of the computed relative energies of various intermediates and transition states along the catalytic cycle. The computed energetics have been found to be in favor of the involvement of a metal alkyl species, as compared to the likely participation of a metal hydride species. The generation of a metal hydride has been identified in the pathway wherein the active catalyst is generated between the pre-catalyst $[M(\eta^3\text{-allyl})(PMe_3)]^+$ and only one molecule of ethylene. However, when two molecules of ethylene are involved in the formation of the active catalyst, a metal alkyl species has been identified as playing the role of the active catalyst. The formation of the metal alkyl species has been found to enjoy an additional stabilizing metal$\cdots H_\beta$ agostic interaction. The inspection of the free energy profiles reveals that the metal alkyl intermediates (in particular **o** and **p**) with a bound olefinic fragment are energetically stable and could, therefore, be amenable to experimental characterization. We anticipate that suitably designed isotopic labeling studies could perhaps help to resolve the identity of the active catalyst in palladium-catalyzed olefin dimerization in the near future. Of the three metal catalysts considered in the present study, cationic Ni(II) is predicted to be the best candidate towards the ethylene dimerization reaction. Amongst the three different density functionals employed for the Ni(II) system, the computed activation barriers at the B3LYP level have generally been found to be higher than those obtained by using the mPW1K and PBE1PBE functionals.

Acknowledgements

Generous computing time from the IIT Bombay computer center is acknowledged. We are thankful to C. B. Shinisha (IIT Bombay) for her help in preparing the revised manuscript.

References and Notes

1 (*a*) X. Domènech, J. A. Ayllón, J. Peral and J. Rieradevall, *Environ. Sci. Technol.*, 2002, **36**, 5517; (*b*) A. Corma and H. Garcia, *Chem. Rev.*,

2002, **102**, 3837; (*c*) P. T. Anastas and M. M. Kirchhoff, *Acc. Chem. Res.*, 2002, **35**, 686; (*d*) T. E. Natan Jr. and C. G. Miller, *Environ. Sci. Technol.*, 1998, **32**, 368A.
2 (*a*) R. Noyori, *Chem. Commun.*, 2005, 1807; (*b*) X. Cui and K. Burgess, *Chem. Rev.*, 2005, **105**, 3272; (*c*) Y. Blum, D. Czarkie, Y. Rahamim and Y. Shvo, *Organometallics*, 1985, **4**, 1459; (*d*) R. H. Crabtree, *Acc. Chem. Res.*, 1979, **12**, 331; (*e*) J. A. Osborn, F. H. Jardine, J. F. Young and G. Wilkinson, *J. Chem. Soc. A*, 1966, 1711.
3 (*a*) O. Diels and K. Alder, *Liebigs Ann.*, 1928, **460**, 98; (*b*) O. Diels and K. Alder, *Liebigs Ann.*, 1929, **470**, 62; (*c*) O. Diels and K. Alder, *Ber.*, 1929, **62**, 2081.
4 K. N. Houk and B. List, *Acc. Chem. Res.*, 2004, **37**, 487.
5 (*a*) A. de Meijere, *Chem. Rev.*, 2000, **100**, 2739; (*b*) M. Schuster and S. Biechert, *Angew. Chem., Int. Ed. Engl.*, 1997, **36**, 2036; (*c*) D. Seebach, *Angew. Chem., Int. Ed. Engl.*, 1990, **29**, 1320.
6 (*a*) R. Chinchilla and C. Nájera, *Chem. Rev.*, 2007, **107**, 874; (*b*) T. A. Barder, S. D. Walker, J. R. Martinelli and S. L. Buchwald, *J. Am. Chem. Soc.*, 2005, **127**, 4685; (*c*) T. V. Rajanbabu, *Chem. Rev.*, 2003, **103**, 2845; (*d*) I. P. Beletskaya and A. V. Cheprakov, *Chem. Rev.*, 2000, **100**, 3009.
7 (*a*) W.-J. Shi, Q. Zhang, J.-H. Xie, S.-F. Zhu, G.-H. Hou and Q.-L. Zhou, *J. Am. Chem. Soc.*, 2006, **128**, 2780; (*b*) M. L. Clarke and G. J. Roff, *Chem.–Eur. J.*, 2006, **12**, 7978.
8 (*a*) J. Joseph, T. V. RajanBabu and E. D. Jemmis, *Organometallics*, 2009, **28**, 3552; (*b*) F. Sauriol, E. Wong, A. M. H. Leung, I. E. Donaghue, M. C. Baird, T. Wondimagegn and T. Ziegler, *Angew. Chem., Int. Ed.*, 2009, **48**, 3342; (*c*) P. Surawatanawong, Y. Fan and M. B. Hall, *J. Organomet. Chem.*, 2008, **693**, 1552; (*d*) S. Tobisch and T. Ziegler, *J. Am. Chem. Soc.*, 2004, **126**, 9059; (*e*) J. J. Carbó, F. Maseras, C. Bo and P. W. N. M. van Leeuwen, *J. Am. Chem. Soc.*, 2001, **123**, 7630; (*f*) S. A. Decker and T. R. Cundari, *Organometallics*, 2001, **20**, 2827.
9 (*a*) A. de Meijere and F. E. Meyer, *Angew. Chem., Int. Ed. Engl.*, 1995, **33**, 2379; (*b*) R. F. Heck, *Org. React.*, 1982, **27**, 345; (*c*) T. Mizoroki, K. Mori and A. Ozaki, *Bull. Chem. Soc. Jpn.*, 1971, **44**, 581.
10 (*a*) M. Kuil, T. Soltner, P. W. N. M. van Leeuwen and J. N. H. Reek, *J. Am. Chem. Soc.*, 2006, **128**, 11344; (*b*) A. Spencer, *J. Organomet. Chem.*, 1980, **194**, 113; (*c*) D. Evans, J. A. Osborn and G. Wilkinson, *J. Chem. Soc.*, 1968, **33**, 3133.
11 (*a*) L. J. Gooßen, *Angew. Chem., Int. Ed.*, 2002, **41**, 3775; (*b*) B. Bogdanović, B. Henc, A. Lösler, B. Meister, H. Pauling and G. Wilke, *Angew. Chem., Int. Ed. Engl.*, 1973, **12**, 954; (*c*) H. Nozaki, S. Moriuti, H. Takaya and R. Noyori, *Tetrahedron Lett.*, 1966, **7**, 5239.
12 (*a*) C. R. Landis and M. D. Christianson, *Proc. Natl. Acad. Sci. U. S. A.*, 2006, **103**, 15349; (*b*) P. Corradini, G. Guerra and L. Cavallo, *Acc. Chem. Res.*, 2004, **37**, 231; (*c*) T. Alderson, E. L. Jenner and R. V. Lindsey Jr., *J. Am. Chem. Soc.*, 1965, **87**, 5638; (*d*) G. Natta and G. Mazzanti, *Tetrahedron*, 1960, **8**, 86.
13 (*a*) J. Flapper, P. W. N. M. van Leeuwen, C. J. Elsevier and P. C. J. Kamer, *Organometallics*, 2009, **28**, 3264; (*b*) R. A. Stapleton, J. Chai, A. Nuanthanom, Z. Flisak, M. Nele, T. Ziegler, P. L. Rinaldi, J. B. P. Soares and S. Collins, *Macromolecules*, 2007, **40**, 2993; (*c*) L. LePichon, D. W. Stephan, X. Gao and Q. Wang, *Organometallics*, 2002, **21**, 1362; (*d*) N. A. Cooley, S. M. Green, D. F. Wass, K. Heslop, A. G. Orpen and P. G. Pringle, *Organometallics*, 2001, **20**, 4769.
14 (*a*) K. Tsuchikama, Y. Kuwata, Y.-K. Tahara, Y. Yoshinami and T. Shibata, *Org. Lett.*, 2007, **9**, 3097; (*b*) M. Hölscher, G. Franciò and W. Leitner, *Organometallics*, 2004, **23**, 5606; (*c*) R. Kumareswaran, M. Nandi and T. V. Rajanbabu, *Org. Lett.*, 2003, **5**, 4345; (*d*) S. A. Decker and T. R. Cundari, *New J. Chem.*, 2002, **26**, 129.
15 N. Nomura, J. Jin, H. Park and T. V. RajanBabu, *J. Am. Chem. Soc.*, 1998, **120**, 459.
16 (*a*) C. T. Burns and R. F. Jordan, *Organometallics*, 2007, **26**, 6726; (*b*) F. C. Rix, M. Brookhart and P. S. White, *J. Am. Chem. Soc.*, 1996, **118**, 4746; (*c*) F. C. Rix and M. Brookhart, *J. Am. Chem. Soc.*, 1995, **117**, 1137.
17 Metal-hydride complexes as well as metal alkyl complexes are proposed to function as active catalysts. For examples see: (*a*) S. Niu and M. B. Hall, *Chem. Rev.*, 2000, **100**, 353; (*b*) S. A. Svejda and M. Brookhart, *Organometallics*, 1999, **18**, 65.
18 (*a*) M. Van Meurs, G. J. P. Britovsek, V. C. Gibson and S. A. Cohen, *J. Am. Chem. Soc.*, 2005, **127**, 9913; (*b*) Y. Luo, J. Baldamus and Z. Hou, *J. Am. Chem. Soc.*, 2004, **126**, 13910.
19 (*a*) S. Noda, A. Nakamura, T. Kochi, L. W. Chung, K. Morokuma and K. Nozaki, *J. Am. Chem. Soc.*, 2009, **131**, 14088; (*b*) V. L. Cruz, J. Ramos, J. Martínez-Salazar, S. Gutiérrez-Oliva and A. Toro-Labbé, *Organometallics*, 2009, **28**, 5889; (*c*) G. Talarico and G. T. Budzelaar, *Organometallics*, 2008, **27**, 4098; (*d*) P. Braunstein, *Chem. Rev.*, 2006, **106**, 134; (*e*) A. B. Dounay and L. E. Overman, *Chem. Rev.*, 2003, **103**, 2945; (*f*) R. Zimmer, C. U. Dinesh, E. Nandanan and F. A. Khan, *Chem. Rev.*, 2000, **100**, 3067; (*g*) E. Negishi, C. Coperet, S. Ma, S.-Y. Liou and F. Liu, *Chem. Rev.*, 1996, **96**, 365.
20 M. J. Frisch, G. W. Trucks, H. B. Schlegel, G. E. Scuseria, M. A. Robb, J. R. Cheeseman, J. A. Montgomery, Jr., T. Vreven, K. N. Kudin, J. C. Burant, J. M. Millam, S. S. Iyengar, J. Tomasi, V. Barone, B. Mennucci, M. Cossi, G. Scalmani, N. Rega, G. A. Petersson, H. Nakatsuji, M. Hada, M. Ehara, K. Toyota, R. Fukuda, J. Hasegawa, M. Ishida, T. Nakajima, Y. Honda, O. Kitao, H. Nakai, M. Klene, X. Li, J. E. Knox, H. P. Hratchian, J. B. Cross, V. Bakken, C. Adamo, J. Jaramillo, R. Gomperts, R. E. Stratmann, O. Yazyev, A. J. Austin, R. Cammi, C. Pomelli, J. Ochterski, P. Y. Ayala, K. Morokuma, G. A. Voth, P. Salvador, J. J. Dannenberg, V. G. Zakrzewski, S. Dapprich, A. D. Daniels, M. C. Strain, O. Farkas, D. K. Malick, A. D. Rabuck, K. Raghavachari, J. B. Foresman, J. V. Ortiz, Q. Cui, A. G. Baboul, S. Clifford, J. Cioslowski, B. B. Stefanov, G. Liu, A. Liashenko, P. Piskorz, I. Komaromi, R. L. Martin, D. J. Fox, T. Keith, M. A. Al-Laham, C. Y. Peng, A. Nanayakkara, M. Challacombe, P. M. W. Gill, B. G. Johnson, W. Chen, M. W. Wong, C. Gonzalez and J. A. Pople, *GAUSSIAN 03 (Revision C.02)*, Gaussian, Inc., Wallingford, CT, 2004.
21 B. J. Lynch, P. L. Fast, M. Harris and D. G. Truhlar, *J. Phys. Chem. A*, 2000, **104**, 4811.
22 (*a*) A. D. Becke, *Phys. Rev. A: At., Mol., Opt. Phys.*, 1988, **38**, 3098; (*b*) A. D. Becke, *J. Chem. Phys.*, 1993, **98**, 5648; (*c*) C. Lee, W. Yang and R. G. Parr, *Phys. Rev. B: Condens. Matter*, 1988, **37**, 785.
23 (*a*) J. P. Perdew, K. Burke and M. Ernzerhof, *Phys. Rev. Lett.*, 1996, **77**, 3865; (*b*) J. P. Perdew, K. Burke and M. Ernzerhof, *Phys. Rev. Lett.*, 1997, **78**, 1396.
24 P. J. Hay and W. R. Wadt, *J. Chem. Phys.*, 1985, **82**, 299.
25 (*a*) R. Álvarez, O. N. Faza, C. S. López and Á. R. de Lera, *Org. Lett.*, 2006, **8**, 35; (*b*) A. Ariafard, Z. Lin and I. J. S. Fairlamb, *Organometallics*, 2006, **25**, 5788; (*c*) G. von Frantzius, R. Streubel, K. Brandhorst and J. Grunenberg, *Organometallics*, 2006, **25**, 118; (*d*) T. Strassner and M. A. Taige, *J. Chem. Theory Comput.*, 2005, **1**, 848; (*e*) H.-P. Wu, D. H. Ess, S. Lanza, T. J. R. Weakley, K. N. Houk, K. K. Baldridge and M. M. Haley, *Organometallics*, 2007, **26**, 3957.
26 (*a*) M. A. Fox, R. L. Roberts, T. E. Baines, B. Le Guennic, J.-F. Halet, F. Hartl, D. S. Yufit, D. Albesa-Jove, J. A. K. Howard and P. J. Low, *J. Am. Chem. Soc.*, 2008, **130**, 3566; (*b*) E. Ben-Ari, R. Cohen, M. Gandelman, L. J. W. Shimon, J. M. L. Martin and D. Milstein, *Organometallics*, 2006, **25**, 3190.
27 (*a*) D. A. Pantazis, J. E. McGrady, M. Besora, F. Maseras and M. Etienne, *Organometallics*, 2008, **27**, 1128; (*b*) G. Talarico, V. Barone, P. H. M. Budzelaar and C. Adamo, *J. Phys. Chem. A*, 2001, **105**, 9014.
28 C. Gonzalez and H. B. Schlegel, *J. Phys. Chem.*, 1990, **94**, 5523.
29 (*a*) A. E. Reed, L. A. Curtiss and F. Weinhold, *Chem. Rev.*, 1988, **88**, 899; (*b*) E. D. Glendening, A. E. Reed, J. E. Carpenter and F. Weinhold, NBO Version 3.1 (Theoretical Chemistry Institute, University of Wisconsin, Madison, WI, 2001).
30 F. Biegler-Konig, J. Schonbohm and D. Bayles, *J. Comput. Chem.*, 2001, **22**, 545.
31 See Table 2 for relative energies computed using the B3LYP and the PBE1PBE density functionals.
32 The computed natural charges (NPA) on phosphorous in **1b**, **TS(1b–1c)**, and **1c** are found to be 0.96, 1.00 and 0.94, respectively.
33 See Table S4 in the ESI† for a list of values for electron density at the Ni···H_β bond critical point.
34 The IRC run from **TS(1d–1e)** results in the formation of an η^1-coordinated Ni–pentadiene complex, **1e′**. This intermediate is found to be 15.7 kcal mol^{-1} higher in energy than **1e**, obtained through an independent geometry optimization, wherein both ends of the pentadiene moiety are coordinated to the Ni atom (η^2 coordination). The improved stability of **1e** arises due to the additional π-coordination between the olefin and coordinatively unsaturated Ni center.
35 The generation of the active catalyst *via* the elimination of 1,4-pentadiene in alkene polymerization has been proposed earlier. An experimental study is reported in: S. Mecking and W. Keim, *Organometallics*, 1996, **15**, 2650 (and references therein for additional details).
36 In spite of repeated attempts, we could not locate any transition state for the expulsion of pentadiene from the metal centers. Similar situations reported in the literature generally endorse the difficulty associated with identifying transition states for olefin coordination and expulsion

from transition metal centers. It is widely known that there is no kinetic barrier for olefin uptake (*i.e.*, conversions such as from **h** to **i**). Some examples include: (*a*) D. M. Philipp, R. P. Muller, W. A. Goddard III, J. Storer, M. McAdon and A. Mullins, *J. Am. Chem. Soc.*, 2002, **124**, 10198; (*b*) F. Bernardi, A. Bottoni and G. P. Miscione, *Organometallics*, 1998, **17**, 16.

37 At the mPW1K level of theory a weak imaginary frequency has been identified for **1h** (–15.6 cm^{-1}). Efforts to eliminate this frequency were unsuccessful. It is further noticed that all the frequencies came out to be positive at the B3LYP level. The small imaginary frequency as noticed in the present case might have been a result of the usage of the default grid size employed by the program. For example, see: B. G. Johnson and M. J. Frisch, *Chem. Phys. Lett.*, 1993, **216**, 133.

38 (*a*) M. J. Calhorda, *Chem. Commun.*, 2000, 801; (*b*) B. O. Roos, R. Lindh, H.-G. Cho and L. Andrews, *J. Phys. Chem. A*, 2007, **111**, 6420.

39 Interestingly, in **1l**, apart from the Ni $\cdots \pi$ interaction, a weak agostic interaction with the free end of the alkene chain is also identified. A transition state **TS(1l–1r)**, implying a facile rotation around the C–C bond of the alkene chain, leading to the formation of another energetically close intermediate **1r**, is identified as well (see Fig. S1 in the ESI†). Thus, either **1l** or **1r** can lead to the formation of active species **1f** *via* 1-butene expulsion..

40 Ethylene oligomerization is generally performed at higher ethylene concentration and high pressure (15–20 bar) conditions; (*a*) M. D. Doherty, S. Trudeau, P. S. White, J. P. Morken and M. Brookhart, *Organometallics*, 2007, **26**, 1261; (*b*) R. Ceder, G. Muller and J. I. Ordinas, *J. Mol. Catal.*, 1994, **92**, 127.

41 The electron density at the bond critical point for this interaction by using the AIM formalism is found to be 0.121 au at the mPW1K/LANl2DZ ECP, 6-311+G** level.

42 G. M. DiRenzo, P. S. White and M. Brookhart, *J. Am. Chem. Soc.*, 1996, **118**, 6225.

43 More details are provided in Table S1 in the ESI†.

44 See Fig. S3 in the ESI† for the optimized geometries of the key stationary points in the Pt(II)-catalyzed ethylene dimerization reaction.

45 See Fig. S2 in the ESI† for the mPW1K computed free energy profile of the Pd(II)-catalyzed ethylene dimerization process.

46 A summary of the energies of all the intermediates and the transition states is provided in Table S1 in the ESI†.

47 It is known that nickel and palladium hydrides exhibit comparable acidities while those of platinum are relatively less acidic; see: C. J. Curtis, A. Miedaner, J. W. Raebiger and D. L. DuBois, *Organometallics*, 2004, **23**, 511.

48 See Table S1 in the ESI† for details on the energies of various stationary points.

49 For some select exampleson metal $\cdots H_\beta$ agostic interaction, see: (*a*) E. Ding, B. Du, F.-C. Liu, S. Liu, E. A. Meyers and S. G. Shore, *Inorg. Chem.*, 2005, **44**, 4871; (*b*) W. Baratta, C. Mealli, E. Herdtweck, A. Ienco, S. A. Mason and P. Rigo, *J. Am. Chem. Soc.*, 2004, **126**, 5549; (*c*) A. C. Cooper, E. Clot, J. C. Huffman, W. E. Streib, F. Maseras, O. Eisenstein and K. G. Caulton, *J. Am. Chem. Soc.*, 1999, **121**, 97.

50 (*a*) U. Koch and P. L. A. Popelier, *J. Phys. Chem.*, 1995, **99**, 9747; (*b*) P. L. A. Popelier, *J. Phys. Chem. A*, 1998, **102**, 1873.

51 (*a*) O. V. Zenkina, A. Karton, D. Freeman, L. J. W. Shimon, J. M. L. Martin and M. E. van der Boom, *Inorg. Chem.*, 2008, **47**, 5114; (*b*) F. Pichierri and Y. Yamamoto, *J. Org. Chem.*, 2007, **72**, 861.

52 (*a*) J. Döbler, M. Pritzsche and J. Sauer, *J. Am. Chem. Soc.*, 2005, **127**, 10861; (*b*) S. Niu, S. Zarić, C. A. Bayse, D. L. Strout and M. B. Hall, *Organometallics*, 1998, **17**, 5139.